Gradiently Alloyed $Zn_xCd_{1-x}S$ Colloidal Photoluminescent Quantum Dots Synthesized via a Noninjection One-Pot Approach

Jianying Ouyang,[†] Christopher I. Ratcliffe,[†] David Kingston,[‡] Baptiste Wilkinson,[†] Jasmijn Kuijper,[†] Xiaohua Wu,[§] John A. Ripmeester,[†] and Kui Yu*,[†]

Steacie Institute for Molecular Sciences, National Research Council of Canada, Ottawa, Ontario K1A 0R6, Canada, Institute for Chemical Process and Environmental Technology, National Research Council of Canada, Ottawa, Ontario K1A 0R6, Canada, and Institute for Microstructural Sciences, National Research Council of Canada, Ottawa, Ontario K1A 0R6, Canada

Received: November 13, 2007

High-quality colloidal photoluminescent (PL) ZnCdS quantum dots (QDs) with gradient distribution of components, consisting of Cd-rich inner cores and Zn-rich outer shells, were synthesized via a noninjection one-pot approach. This newly developed synthetic approach uses zinc stearate ($Zn(St)_2$), cadmium acetate dihydrate ($Cd(OAc)_2{\cdot}2H_2O$), and elemental sulfur as Zn, Cd, and S source compounds, respectively. The growth of the cubic-structured QDs was carried out at 240 °C in a reaction flask consisting of the source compounds, together with stearic acid (SA), 2,2′-dithiobisbenzothiazole (MBTS), and 1-octadecene (ODE); all of these chemicals were loaded at room temperature. The temporal evolution of the optical properties of the growing QDs, including absorption and photoemission, was monitored in detail; the evolution monitored indicates that the growth kinetics, the composition, and the distribution of the Zn and Cd in the resulting ternary $Zn_xCd_{1-x}S$ QDs are sensitive to feed Zn−Cd−S molar ratios. Detailed investigation on the feed Zn−Cd−S molar ratio affecting the QD growth and optical property was performed, together with detailed structural characterization by solid-state NMR including cross polarization (CP) and dipolar dephased cross polarization (DDCP); also, the resulting QDs were characterized by XPS, TEM, and XRD. Accordingly, the synthesis-structure−property relationship was explored systematically. Tuning the feed Zn−Cd−S stoichiometry, high-quality $Zn_xCd_{1-x}S$ QDs exhibiting sharp excitonic absorptions, narrow PL emissions with full width at half-maximum (fwhm) on the order of 19−21 nm, and high PL quantum yield (QY, up to 23%), could be fabricated with relatively low Zn and S feed amount, such as 1Zn−1Cd−1S feed molar ratio. In general, our noninjection approach features great synthetic reproducibility and is easy to scale up, with a plausible alloying mechanism of the formation of a Cd-rich core in the early growth stage, followed by a gradual formation of Zn-rich outer layers with increasing zinc content toward the surface.

1. Introduction

Colloidal photoluminescent (PL) semiconductor nanocrystals have attracted significant attention over the past decade due to their fascination in both fundamental science and potential applications. When the size of spherical semiconductor nanocrystals becomes less than or comparable to that of a photogenerated exciton in bulk materials, they are so-called quantum dots (QDs). Efforts on QDs are devoted to understanding the evolution of material characteristics from molecules, to nanoclusters, and to bulk materials;[1] also, efforts are dedicated to exploring the applications of QD-based nanomaterials,[2,3] such as bio-imaging with nanomaterial intrinsic characteristics overcoming the limitations of traditional fluorescent molecules. Among II−VI colloidal QDs, cadmium selenide (CdSe) QDs are probably the most extensively investigated regarding the development of synthetic routes with robust surface passivation[4] and ligand dynamics,[5] together with photophysics[6] and modeling.[7] Meanwhile, cadmium sulfide (CdS) QDs are probably the second most extensively studied system. CdS has a bulk band gap of 2.48 eV[8] (ca. 500 nanometers (nm)) with its exciton Bohr radius of 3.0 nm;[9] therefore, CdS QDs are good candidates as blue emitters, when their sizes are in the range of 3.4−6.5 nm with their corresponding PL emission thus in the blue wavelength range of 420−490 nm,[10] according to the international standard for primary colors, namely CIE Chromaticity Diagram established in 1931 by the Commission Internationale d'Eclairage (CIE).

In addition to the size control for the tuning capability of the optical properties of binary QDs, recent advances in synthesis have led to the exploration of ternary QDs with tunable optical properties by changing their constituent stoichiometries as well as their internal structure. For homogeneous ternary QDs, both the confinement potential and the interfacial strain change with their composition; thus, the band gap energy can be tuned even at a constant size. Ternary colloidal ZnCdS QDs are excellent candidates as blue emitters. For zincblende ZnS and CdS, their lattice constants at room temperature are 5.406 and 5.835 Å, respectively;[8] such a low lattice mismatch promises that the introducing of Zn into the CdS lattice to form ZnCdS alloyed QDs is a practical way to engineer blue emitters with high band gap emission efficiency. It is noteworthy that Zn is a nontoxic

* To whom correspondence should be addressed.
[†] Steacie Institute for Molecular Sciences.
[‡] Institute for Chemical Process and Environmental Technology.
[§] Institute for Microstructural Sciences.

10.1021/jp710852q CCC: $40.75 Published 2008 by the American Chemical Society
Published on Web 03/05/2008

element, and bulk ZnS has a band gap energy of ~3.7 eV at room temperature[8] (ca. 335 nm) with its exciton Bohr radius of 2.2 nm.[11]

The non-organometallic synthesis of high-quality CdS QDs, regarding the control of the size and size distribution as well as band gap PL and deep-trapping PL, was successfully achieved only recently. In 2002, a hot-injection approach in a noncoordinating solvent octadecene (ODE) was reported, together with the presence of oleic acid (OA);[12] after a couple of years, another hot-injection synthesis but in a coordinating long-chain amine was published.[13] In the same year 2004, a unique noninjection one-pot approach was reported, with the presence of two compounds, namely tetraethylthiuram disulfides and 2,2′-dithiobisbenzothiazole, to separate nucleation and growth stages in a homogeneous reaction system.[14] In all of the three successful approaches, air-stable CdO or cadmium salts as well as elemental sulfur were used as Cd and S source compounds, respectively, instead of hazardous $Cd(CH_3)_2$ and $(TMS)_2S$.[4a] It is worth mentioning that the use of air-stable chemicals continues the trend toward "greener" syntheses of high-quality colloidal QDs,[15] which was first achieved in 2001, with CdO replacing $Cd(CH_3)_2$.[4c]

At the same time, there is a limited body of literature on wet-chemistry approaches to colloidal PL alloyed ZnCdS QDs and little detailed information on their synthesis−structure−property relationships. ZnS−CdS co-colloids prepared by aqueous precipitation was reported in the 1980s[16] while nanocrystalline ZnCdS by a chemical reduction route in 2002,[17] but they both exhibited poor optical properties. Colloidal ZnCdS QDs exhibiting reasonable optical properties with blue emission were reported in 2003; they were synthesized via a hot-injection approach and characterized as wurtzite nanocrystals with varied compositions, sizes, as well as narrow size distribution.[18] The hot-injection approach was carried out in ODE, with CdO/OA and ZnO/OA complexes as Cd and Zn precursors, respectively, and elemental sulfur as S precursor. Such an approach bears similarity to that used in the synthesis of CdS QDs in ODE,[12] comprising of a swift injection of a solution of S in ODE into an ODE solution consisting of the CdO/OA and ZnO/OA complexes at 300 °C. Furthermore, colloidal alloyed ZnCdS QDs, which were zincblende with different compositions, were synthesized in coordinating long-chain amines via a hot-injection approach.[13] Such an approach involved a swift injection of a solution of elemental sulfur in dodecylamine (DDA) into a solution of cadmium stearate ($Cd(St)_2$) and zinc stearate ($Zn(St)_2$) in hexadecylamine (HDA) at 270 °C.[13] The two hot-injection approaches were reported to produce homogeneous ternary ZnCdS QDs.[13,18] To the best of our knowledge, there is no literature report on noninjection approaches to synthesize colloidal PL ZnCdS QDs.

It is easy to understand that hot-injection-based synthetic methods are not suitable for large-scale production of high-quality QDs with narrow size distribution.[14] In order to separate the nucleation and growth stages for tight size distribution, the hot-injection approach requires rapid injection of a precursor solution, fast decrease of the reaction temperature right after the injection, and strong stirring for efficient mass transfer; the realization of these requirements is not easy at large-scale production. Accordingly, the development of noninjection-based synthetic approaches is in demand.

This manuscript, focusing on the synthesis-structure−property relationship, reports a noninjection one-pot approach to readily synthesize high-quality colloidal PL ZnCdS QDs, together with detailed characterization on the structures and optical properties of the resulting ZnCdS QDs. This noninjection approach is easily scaled up, with great synthetic reproducibility, using zinc stearate ($Zn(St)_2$), cadmium acetate dihydrate ($Cd(OAc)_2{\cdot}2H_2O$), and elemental sulfur as Zn, Cd, and S source compounds, respectively. Feed Zn−Cd−S molar ratios significantly affect the growth kinetics, the composition, and the distribution of the Zn and Cd of the resulting ternary $Zn_xCd_{1-x}S$ QDs. With relatively high Zn and S feed amounts, such as 3Zn−1Cd−4S, the temporal evolution of the spectral absorption and emission of the growing ZnCdS QDs is unique, with fixed and even blue-shifted absorption and emission peaks after an initial red-shifting in the first a few minutes of growth at 240 °C. These unusual optical properties prompted us to investigate the structures of the resulting ternary ZnCdS QDs. In contrast to the homogeneous alloys usually reported in the hot-injection approaches,[13,18] our cubic-structured ZnCdS QDs have a gradient distribution of components consisting of Cd-rich inner cores and Zn-rich outer layers as revealed by solid-state NMR and XRD. With low Zn and S feed amounts (such as 1Zn−1Cd−1S), the resulting $Zn_xCd_{1-x}S$ QDs exhibited sharp exciton absorptions, narrow PL emissions with full width at half-maximum (fwhm) on the order of 19−21 nm, and high PL quantum yield (up to 23%).

2. Experimental Section

All of the chemicals used are commercially available and were used as received. They are cadmium acetate dihydrate ($Cd(OAc)_2{\cdot}2H_2O$, Alfa Aesar, 99.999%), zinc stearate ($Zn(St)_2$, with 12.5−14% ZnO, Alfa Aesar), elemental sulfur (S, Anachemia, precipitated), stearic acid (SA, Aldrich, 98+%), 2,2′-dithiobisbenzothiazole (MBTS, Aldrich, 99%), and 1-octadecene (ODE, Aldrich, tech. 90%). For the Cd source compound, a simple abbreviation of $Cd(OAc)_2$ will be used in our text below.

In a typical synthesis with an equimolar feed ratio of 1Zn−1Cd−1S, S (3.4 mg, 0.11 mmol), MBTS (2.5 mg, 7.40 μmol), and ODE (~3.0 g) were sonicated together for 1 h; afterward, this dispersion was added into a three-necked round-bottom flask containing $Zn(St)_2$ (0.10 mmol), $Cd(OAc)_2$ (0.11 mmol), SA (0.33 mmol), and ODE (~2.5 g) at room temperature. Afterward, the mixture with a total ODE of ca. 5.5 g was heated up to 120 °C with stirring under vacuum (~30 mTorr). A clear solution was obtained after ca. 2 h. The resulting solution was further heated up to 240 °C at a rate of ca. 10 °C/min under a flow of purified nitrogen. The growth time was counted once the temperature reached 240 °C, and this temperature was kept constant for the growth/annealing process of the ZnCdS QDs. Such a synthetic protocol bears similarity to that used in the synthesis of zincblende CdS QDs in ODE.[14]

To monitor the temporal evolution of the optical properties of the QD growth, small aliquots (~ 0.2 mL) of the reaction mixture were quickly taken at ~200 °C, ~225 °C, and 240 °C and at different time intervals of 1, 2, 4, 8, 20, 45, 90, 120, and 180 min at 240 °C. Usually, 30 μL of the raw reaction aliquots was dispersed in 3 mL of hexanes (Hex), and the absorption and emission spectra of Hex dispersions were collected at room temperature. Optical absorption spectra were collected with a Perkin-Elmer Lambda 45 ultraviolet−visible (UV−vis) spectrometer using a 1-nm data collection interval. Photoemission experiments were performed on a Fluoromax-3 spectrometer (Jobin Yvon Horiba, Instruments SA), with a 450 W Xe lamp as the excitation source, an excitation wavelength of 350 nm (if not specified), an increment of data collection of 2 nm (if not specified), and the slits for excitation and emission of 3 nm (if not specified). For the emission peak, baseline-subtracted

TABLE 1: Structural Characterization of the Binary CdS and Ternary $Zn_xCd_{1-x}S$ Nanocrystals Synthesized via Our Noninjection Approach but with Large-Scale

feed molar ratio	1Cd-1S	1Zn−1Cd−1S	3Zn−1Cd−2S		3Zn−1Cd−4S	
growth time at 240 °C	180 min	180 min	8 min	180 min	8 min	180 min
first excitonic absorption peak positions	440.0 nm	421.5 nm	409.7 nm	411.1 nm	399.2 nm	395.7 nm
PL band gap emission peak positions/fwhm	452.3/20.5 nm	433.3/22.2 nm	422.1/16.2 nm	422.8/24.9 nm	413.2/18.3 nm	413.4/21.4 nm
atomic compositions by XPS	CdS	Zn0.13Cd0.87S	Zn0.12Cd0.88S	Zn0.36Cd0.64S	Zn0.52Cd0.48S	Zn0.66Cd0.34S
(220) 2θ positions[a]	44°	44.04°	44.04°	44.57°	44.77°	45.77°
estimated mean sizes from XRD[b]	4.91 nm	4.65 nm	3.98 nm	3.88 nm	3.71 nm	4.26 nm
measured mean sizes from TEM	4.2 nm		4.0 nm	3.7 nm	3.5 nm	4.1 nm
^{113}Cd MAS NMR chemical shifts[c]	808 ppm		808 ppm	822 ppm	832 ppm	855 ppm
^{113}Cd CP MAS NMR surface Cd chemical shifts	457 ppm		458 ppm	∼468 ppm	not detected	not detected

[a] Fitted peak positions after a deconvolution of the diffraction peaks of (220) and (311) in the XRD spectra. [b] Calculated by the Sherrer equation[24] using the fitted full width of half-maximum (fwhm) of the diffraction peak (220) in the XRD spectra, with the assumption of no microstrains in the ternary systems. [c] Bulk wurtzite CdS at 805.7 ppm.[21d]

and Gaussian-fitted integration was performed, with a built-in Fluoromax-3 software, to yield the peak position, full width at half-maximum (fwhm), and peak area for the calculation of quantum yield (QY). PL QY was determined by comparing the integrated emission of a given QD sample in dilute hexane dispersion with that of quinine sulfate in 0.05 M H_2SO_4 (Lit. QY ∼ 0.546).[4a,19] The optical density at the excitation wavelength was ∼0.1. Corrections were made for the refractive index differences of solvents.[18]

Intense purification of QD samples was carried out for the characterization of transmission electron microscopy (TEM), X-ray photoelectron spectroscopy (XPS), solid-state nuclear magnetic resonance (NMR), and powder X-ray diffraction (XRD). It is necessary to point out that large-scale syntheses (8−16 times that of typical synthesis described above) were carried out for the structural characterization listed in Table 1. TEM was performed on a JEOL JEM-2100F electron microscope operating at 200 kV and equipped with a Gatan UltraScan 1000 CCD camera. The samples were prepared by drying dilute purified QD dispersions in chloroform onto 300-mesh carbon-coated TEM copper grids. XPS was performed using a Kratos Axis Ultra XPS equipped with a monochromated Al X-ray source. The takeoff angle was 54°. The purified QDs were deposited and dried on silicon wafer substrates; afterward, the substrate was mounted with doubled-sided copper tape. All analyses were calibrated to C 1s at 285 eV. Our purified ZnCdS QDs failed to be analyzed by ICP-AES (Inductively coupled plasma-atomic emission spectrometry), due to the fact that the QDs could not be digested completely by the mixture of concentrated hydrochloric acid and nitric acid (3/1, v/v). Solid-state NMR spectra were obtained on a Bruker AMX300 spectrometer with a Doty Scientific Inc. 5 mm probe using silicon nitride rotors.[20] ^{113}Cd NMR magic angle spinning (MAS) spectra were obtained at 66.58 MHz, both with and without ^{1}H cross-polarization (CP). For spectra without CP a simple one pulse sequence with phase cycling was used, with a 90° pulse length of 4.0 ms and spin rates from 6.3 to 7.3 kHz. A recycle time of 120 s was used and collection times were of the order of 1.5−2.75 days. ^{113}Cd CP/MAS spectra were obtained with CP times of 5−15 ms, recycle times of 1−2 s, and collection times of 7−44 h. Chemical shifts were referenced to $Cd(NO_3)_2 \cdot 4H_2O$ (powdered, under MAS). Standard ^{13}C CP/MAS spectra at 75.43 MHz were obtained with a CP time of 3 ms, and 4 s recycle times, and dipolar dephasing spectra were obtained with an interruption of ^{1}H decoupling of 40 μs before data acquisition (referenced to TMS via external hexamethylbenzene). Powder X-ray diffraction (XRD) patterns were recorded at room temperature on a Bruker Axs D8 X-ray diffractometer using Cu Kα radiation in a $\theta-\theta$ mode. The generator was operated at 40 kV and 40 mA, and data were collected between 5° and 80° in 2θ with a step size of 0.1° and a counting time of 5 s per step. XRD samples were prepared by depositing the purified nanocrystals on low-background quartz plates.

3. Results and Discussion

In the field of photoluminescent colloidal II−IV QDs, ternary systems, such as CdSeS, CdTeSe, ZnCdSe, and ZnCdS alloys, are attractive. The alloyed nanocrystals can exhibit unusual optical properties as compared to their binary counterparts; meanwhile, without the change of their sizes, they can exhibit various emission colors and PL efficiencies with the modification of their compositions and/or their internal structures such as homogeneous or gradient alloys.[20,21] For example, alloyed CdSeS nanocrystals can be readily tuned to emit in the range of 480 to 540 nm, the emission window of which is not easily achieved with binary CdS or CdSe QDs alone.[21a,b] Also, homogeneously alloyed CdTeSe nanocrystals emit at considerably lower energies than similarly sized binary CdSe and CdTe QDs due to the optical bowing phenomenon[21c] and an nearly 50-fold increase of PL efficiencies was found in gradient CdTeSe alloyed QDs, with the center region rich in Te and the outer shell rich in Se, as compared to homogeneous CdTeSe alloys.[20] Meanwhile, ZnCdSe alloyed QDs can exhibit comparable photoluminescent properties in comparison to CdSe-based QDs.[21d,e]

Our report focuses on the synthesis-structure−property relationship of colloidal ZnCdS alloyed QDs exhibiting photoemission in the blue spectral region. Accordingly, the results and discussion section consists of two parts: the investigation on the growth of the ZnCdS nanocrystals synthesized via our noninjection approach is presented in the first part; the structural characterization of the resulting alloyed ZnCdS QDs is dealt with in the second part, together with a discussion on the alloying mechanisms. The photostability and storage-stability of the resulting ZnCdS QDs are addressed in Supporting Information.

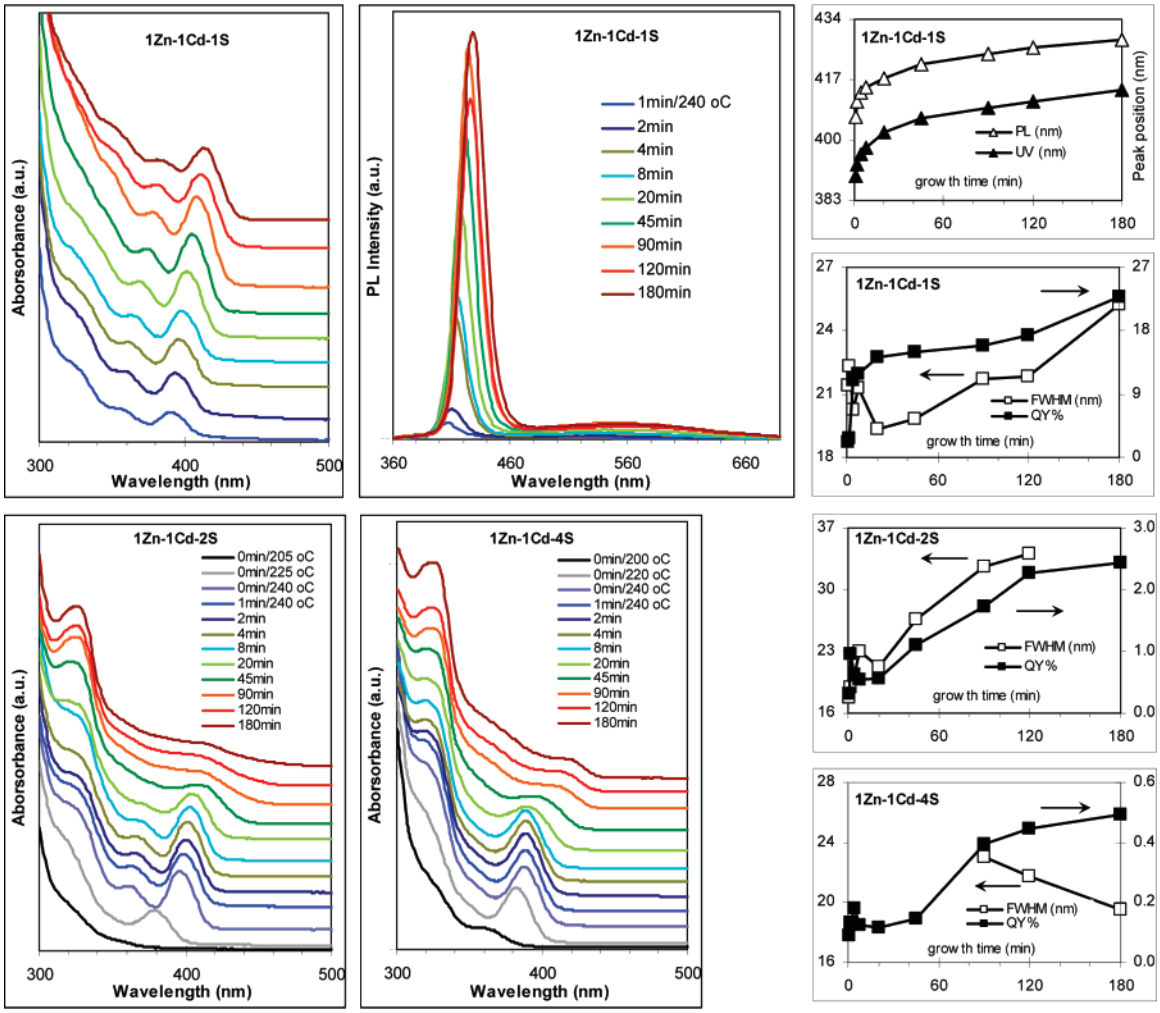

Figure 1. (Top panel) Temporal evolution of the UV−vis absorption spectra (left, offset) and photoluminescent (PL) emission spectra (middle) of the growing ZnCdS nanocrystals from the synthetic batch with the feed molar ratio of 1Zn−1Cd−1S. The nanocrystals with the different growth periods (in minutes as indicated) are represented by different colors. The PL excitation wavelength was 350 nm. Temporal evolution of the band gap peak positions of the absorption (■) and emission (□), and PL QY (■) and PL fwhm (□) is also summarized (right). (Bottom panel) Temporal evolution of the UV−vis absorption spectra of the growing ZnCdS nanocrystals from the synthetic batches with the feed molar ratio of 1Zn−1Cd−2S (left, offset) and 1Zn−1Cd−4S (middle, offset). The nanocrystals with the different growth periods (in minutes as indicated) are represented by different colors. Temporal evolution of the PL QY (■) and PL fwhm (□) is also summarized (right). The nanocrystals from the 1Zn−1Cd−2S feed molar ratio with the growth period of 180 min and those from the 1Zn−1Cd−4S feed molar ratio with the growth periods less than 90 min have not been shown PL fwhm, because of an ambiguity in the determination, arising from the fact of very low band gap PL intensity and very high deep-trap emission intensity.

3.1. Temporal Evolution of the Optical Properties of Growing ZnCdS Nanocrystals. Our noninjection approach features relatively mild synthetic conditions and high reproducibility with large-scale capability, as compared to the existing hot-injection approaches.[12,13,18] It is known that the temporal evolution of the optical properties consisting of absorption and emission is indicative of the formation and growth kinetics of nanocrystals. Thus, the growth of the ZnCdS QDs from our noninjection approach was monitored in terms of the temporal evolution of their optical properties. Various synthetic parameters and the interplay between them affect the growth. This manuscript addresses the Zn−Cd−S feed ratio affecting the growth: with different feed molar ratios of the three source components, the resulting ZnCdS QDs exhibit various behaviors of the temporal evolution of the optical properties due to their sizes and compositions.[22] For example, with relatively high Zn and S feed ratios, the growing ZnCdS nanocrystals exhibit band gap absorption and photoemission at a constant or slightly blueshifted wavelength with a continuous increase in quantum yield. Thus, in this session, we address the ZnCdS QDs from synthetic batches with varied S feed molar ratios, first at an equal Zn-to-Cd feed molar ratio and afterward high Zn-to-Cd feed molar ratios.

3.1.1. Equal Zn-to-Cd Feed Molar Ratio of 1Zn−1Cd−yS with y = 1, 2, and 4. ZnCdS nanocrystals were prepared from synthetic batches with an equal Zn-to-Cd feed molar ratio but different S molar ratios, namely 1Zn−1Cd−*y*S, where $y = 1$, 2, and 4. Basically, these growing QDs exhibited an increase in their band gap PL efficiency with growth time; however, the QDs from the three batches were different, regarding the intensity ratio of the band gap emission to deep-trapping emission. The growing ZnCdS QDs from the 1Zn−1Cd−1S batch exhibited dominant band gap emission with deep-trapping emission highly suppressed, whereas those from the 1Zn−1Cd−2S and 1Zn−1Cd−4S batches exhibited significant deep-trapping emission. The temporal evolution of the absorption and corresponding PL emission of the growing QDs from the synthetic batch with a feed molar ratio of 1Zn−1Cd−1S is shown in Figure 1 (top panel), while the absorption of those from 1Zn−1Cd−2S and 1Zn−1Cd−4S feed molar ratios are

given in Figure 1 (Bottom Panel). The temporal evolution of the peak positions of the first excitonic absorption and band gap PL emission, the PL fwhm, and quantum yield in hexanes, are also summarized in Figure 1. The comparison of the temporal evolution of the optical properties of the nanocrystals from the feed molar ratio of 1Zn−1Cd−(1−4)S is described below, in the order of increasing S molar ratios.

For the growing ZnCdS QDs from the synthetic batch with the feed molar ratio of 1Zn−1Cd−1S (Figure 1, top panel), during the growth period of 1−180 min at 240 °C, the first excitonic absorption peaks exhibit significant red shifts from 390 to 414 nm, and the corresponding PL band gap emission peaks from 407 to 428 nm. These growing QDs are narrow in size distribution, as suggested by their rich absorption fine substructures and the PL fwhm (19−21 nm). It is important to point out that the narrow PL fwhm of our ZnCdS QDs does not result from the weak quantum confinement effect (QCE),[18] due to their relatively small sizes (see TEM characterization) as compared to the corresponding Bohr radius (typical exciton Bohr radii of ZnS and CdS are 2.2 and 3.0 nm[9,11]). Regarding the quantum yield (QY) of the band gap PL emission, the 1−180 min growing ZnCdS QDs exhibit a steady increase from 2.2% to 22.8%; such a QY value of the 180-min QD ensemble is comparable to that reported for the best ZnCdS alloys which were obtained via the hot-injection approach; for example, 25−50% QY (with PL fwhm of 14−18 nm) was reported for the ZnCdS QDs with oleic acid as surface ligands,[18] while 25−45% QY (with PL fwhm in the range of 29−38 nm) was reported for those with hexadecylamine (HDA) as surface ligands.[13] It is necessary to point out that, during the temperature increasing from 120 to 240 °C at 10 min/°C, there was no nanocrystal formation monitored below 200 °C; only till ∼220−230 °C, the nanocrystals started to form.

For the growing ZnCdS QDs from 1Zn−1Cd−2S feed molar ratio (Figure 1, bottom panel), no absorption was detected till 200 °C, followed by the appearance of a distinctive first excitonic peak at 379 nm at 225 °C, with this peak quickly red shifting to 397 nm at 240 °C. This initial growth pattern between 200 and 240 °C was also found in the synthetic batches with other Zn−Cd−S feed molar ratios. During the growth period of 1−20 min at 240 °C, they exhibited slightly redshifting first excitonic absorption and PL band gap emission. After 20 min, their absorption becomes broad with a decrease of the optical density and an increase in PL fwhm. The growing QDs exhibit an increase in QY with a maximum value of 2.4% for the 180-min nanocrystals. For the growing ZnCdS QDs from a feed molar ratio of 1Zn−1Cd−4S, they exhibited little redshifting band gap absorption during the growth period of 1−8 min at 240 °C following the quick growth from 200 to 240 °C. A significant redshift in the absorption is observed with peak broadening and a decrease of the optical density after 8 min. The growing QDs exhibit an increase in QY with a maximum value of 0.5% for the 180-min nanocrystals.

3.1.2. High Zn-to-Cd Feed Molar Ratios of 3Zn−1Cd−yS and 6Zn−1Cd−6S. In order to synthesize ZnCdS QDs with high band gap energy, high Zn-to-Cd feed molar ratios were used, due to the fact that Zn is less reactive toward S than Cd. The Zn composition in the resulting nanocrystals is expected to increase with the increase of the Zn-to-Cd feed molar ratio and the S feed amount. ZnCdS QDs were thus prepared from five synthetic batches with 3Zn−1Cd−yS feed molar ratios, where $y = 1$, 2, 4, and 8, and with 6Zn−1Cd−6S feed molar ratio. Basically, these growing QDs exhibited dominant band gap emission with deep-trapping emission highly suppressed, except those from the 3Zn−1Cd−8S batch with significant deep-trapping emission. Figure 2 shows the temporal evolution of the absorption and corresponding PL emission of the growing QDs with the feed molar ratios of 3Zn−1Cd−1S (a), 3Zn−1Cd−2S (b), 3Zn−1Cd−4S (c), and 6Zn−1Cd−6S (d). The peak positions of the band gap absorption and emission, the PL fwhm, and quantum yield in hexanes are also summarized for the growing ZnCdS QDs prepared from the five batches (see the Supporting Information). The comparison of the temporal evolution of the optical properties of the nanocrystals from these five synthetic batches is described below, in the order of increasing Zn-to-Cd feed molar ratio and S molar ratio.

The growing ZnCdS QDs from the synthetic batch with the feed molar ratio of 3Zn−1Cd−1S (less S to metals) exhibit the temporal evolution of their optical properties similar to that of those from 1Zn−1Cd−1S feed molar ratio, with steady redshifts of the first excitonic absorption peak (390−433 nm) and of the corresponding narrow band gap emission peak (407−446 nm, PL fwhm 16−22 nm) during the 1−80 min growth at 240 °C after the quick growth from 200 to 240 °C. The quantum yield of band gap PL emission increases to a maximum value of 6.2% at 20 min and maintained afterward. Likewise, the growing ZnCdS QDs from 3Zn−1Cd−2S feed molar ratio show similar temporal evolution of their optical properties till 45 min, exhibiting fine absorption substructures and small PL fwhm of 19−21 nm, with the redshifts of their band gap absorption and emission. Afterward, the band gap absorption and emission became broad, together with a decrease of the optical density. It is interesting that the absorption peak gradually blueshifted about 6 nm during the 45−180 min growth, whereas the PL emission peak shifted little at ca. 427 nm. Two factors can possibly lead to the blueshift observed, namely the decrease in size and/or the increase of the Zn content in the CdS crystal lattice resulting in the compression of the lattice. As shown below (see Figure 3 TEM), the size changes little without reduction during the 1−180 min reaction; accordingly, the blueshift is mainly due to the Zn diffusion into the CdS lattice.

For the growing ZnCdS QDs from 3Zn−1Cd−4S feed molar ratio (equal S to metals), a unique quick "fixation" of both the band gap absorption (at 402 nm) and emission (at 415 nm) is pronounced after a small redshift (3 nm) in the initial a couple of minutes at 240 °C. A small blueshift (∼ 2 nm) of absorption was observed after 90 min. These growing ZnCdS nanocrystals exhibited less absorption fine substructures, as compared to those from the 3Zn−1Cd−(1−2)S batches, but still with relatively narrow PL fwhm on the order of 18−23 nm. They exhibited a steady increase in PL QY up to a maximum value of 3.5% at 180 min. A separate experiment, in which the reaction time was extended to 24 h at 240 °C, showed no further blueshifts of the band gap absorption and emission after 180 min, thus the equilibrium of the ternary structure is established in 180 min.

For the growing ZnCdS QDs from 3Zn−1Cd−8S feed molar ratio (excess S to metals, spectra not shown), the quick 'fixation' of both the band gap absorption (at 389 nm) and emission (at 404 nm) is apparent, which is similar to those from 3Zn−1Cd−4S. These QDs exhibited PL fwhm on the order of 30−37 nm and low QY with a maximum value of 0.7% for the 180-min ensemble. Accordingly, the more the S feed amount in the 3Zn−1Cd−yS batches, the larger the band gap of the ZnCdS QDs. However, an excess S-to-metals feed molar ratio impedes the development of band gap emission, as also shown in the previous 1Zn−1Cd−yS batches, and has a negative influence on the optical properties of the resulting QDs, regarding a large intensity ratio of deep-trapping emission to band gap emission.

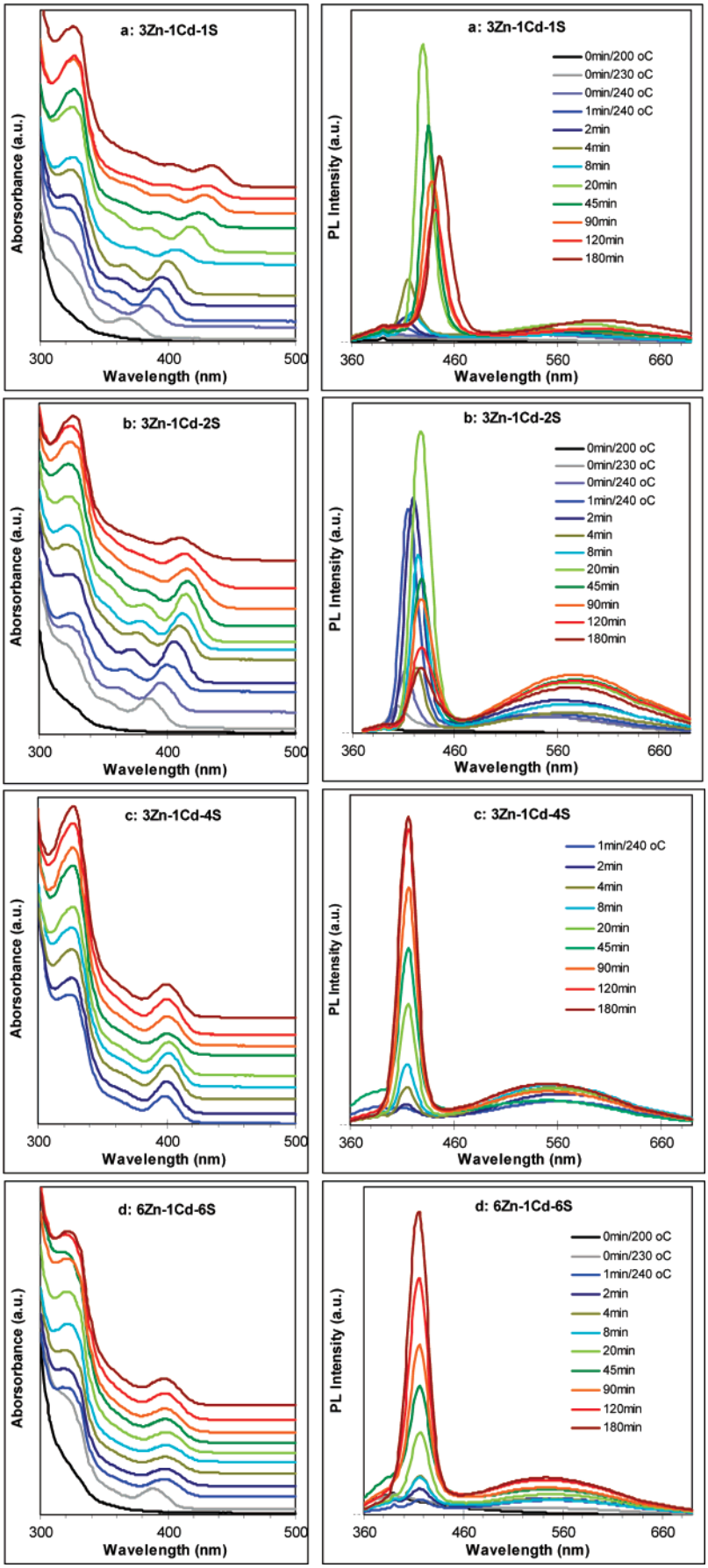

Figure 2. Temporal evolution of the UV−vis absorption spectra (left, offset) and photoluminescent (PL) emission spectra (right) of the growing ZnCdS nanocrystals from the synthetic batches with the feed molar ratio of (a) 3Zn−1Cd−1S, (b) 3Zn−1Cd−2S, (c) 3Zn−1Cd−4S, and (d) 6Zn−1Cd−6S. The nanocrystals with the different growth periods (in minutes as indicated) are represented by different colors. The PL excitation wavelength was 350 nm.

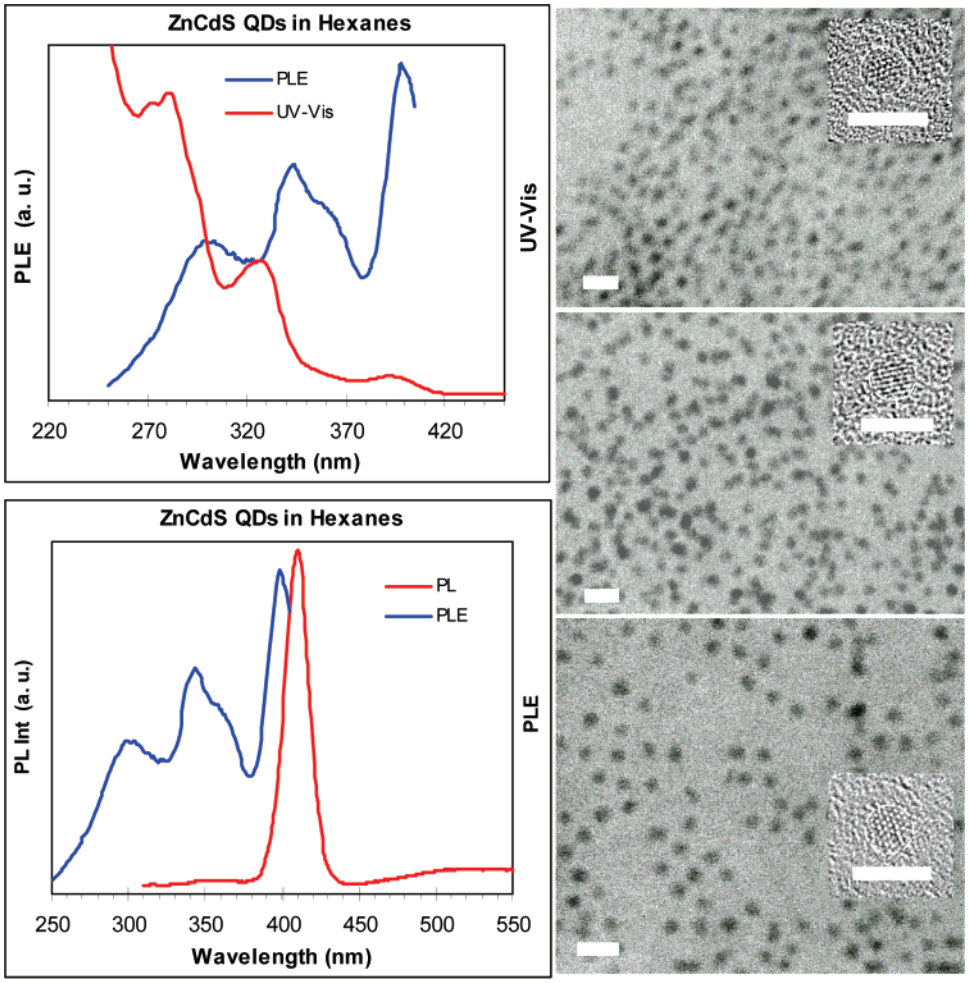

Figure 3. (Right) Photoluminescent excitation (PLE) spectrum (in blue) with the emission at 411 nm for hexanes dispersion of 180-min ZnCdS QDs from 3Zn−1Cd−4S feed molar ratio in a large-scale synthesis. The corresponding UV−vis absorption (up in red) and PL emission (down in red, excitation 300 nm) spectra are also presented. (Left) TEM images of (top) 8-, (middle) 45-, and (bottom) 180-min ZnCdS nanocrystals from the synthetic batch with the feed molar ratio of 3Zn−1Cd−4S. The samples are the same as those shown in Figure 2c. The scale bar is 10 nm. The insert in each TEM image is one corresponding high-resolution TEM image showing the crystal fringes with the scale bar of 5 nm.

This negative influence may be because more Zn can be introduced into the CdS crystal lattice with a relatively high S feed ratio, thus causing more defects and a lower crystallinity due to the lattice mismatch. Therefore, a relatively low S feed ratio is preferred for high-quality ZnCdS QDs.

In order to prepare ZnCdS nanocrystals with a large band gap, the synthesis with an even higher Zn-to-Cd feed molar ratio was conducted without excess of S feed amount, i.e., 6Zn−1Cd−6S. The resulting QDs exhibited the temporal evolution of the optical properties, very much similar to that from the 3Zn−1Cd−4S batch. The 'fixation' of both the band gap absorption (at 398−401 nm) and emission (at 415−417 nm) is obvious after the quick growth from 200 to 240 °C. There is a continuous enhancement in PL QY with the maximum of 4.4% for the 180-min ensemble. The PL fwhm is on the order of 24−27 nm, which is larger than that of the 3Zn−1Cd−4S batch. Since the absorption and emission peak positions of ZnCdS QDs from the 6Zn−1Cd−6S batch are nearly identical to those from the 3Zn−1Cd−4S batch, we can conclude that 3Zn-to-1Cd is sufficient, higher than this ratio like 6Zn-to-1Cd cannot introduce significantly more Zn into the CdS crystal lattice. Hence, we conclude that, with our noninjection approach, a high Zn-to-Cd feed molar ratio and an equal metals-to-S feed molar ratio lead to large band gap high-quality ZnCdS QDs exhibiting dominant band gap emission and highly suppressed deep-trapping emission; furthermore, the QDs exhibit an enhancement in quantum efficiency with almost fixed band gap absorption and emission during the hours of growth at 240 °C. Such a unique pattern of the temporal evolution of the optical properties of the growing QDs suggests a high-level experimental control of the subtle balance between the growth in size and the Zn content increase in the CdS crystal lattice.

It is easy to rule out the separate nucleation and formation of binary CdS and ZnS QDs in our noninjection approach. As shown above, the growing QDs usually exhibit single band gap emission peak with small PL fwhm. There may be concerns about the big absorption feature around 325 nm, which presents in all feed molar ratios of Zn−Cd−S but 1Zn−1Cd−1S as seen in Figures 1 and 2. In order to elucidate its nature, the photoluminescent excitation (PLE) spectrum was recorded with the emission at 411 nm for one nanocrystal ZnCdS ensemble dispersed in hexanes; this ensemble was from a large-scale synthesis with the feed molar ratio of 3Zn−1Cd−4S and 180-min growth. The PLE spectrum together with the corresponding UV−vis absorption and PL emission (exited at 300 nm) are presented in Figure 3 (left). It is clear that, with the excitation at 300 nm, the ZnCdS ensemble exhibits a single PL emission peak at 411 nm, which is due to the band gap photon absorption at 394 nm. After purification, actually, no absorption peak was observed around 270 ∼ 280 nm, the range of which is the

absorption of cadmium stearate and cadmium myristate;[12] also, no absorption peak was detected around 325 nm. Interestingly, the absorption feature around 325 nm is also found in the syntheses of binary CdS with excess feed S to $Cd(OAc)_2$ and of binary ZnS with similar experimental setup. So it is not reasonable to attribute this absorption to either magic-sized CdS nanoclusters or ZnS QDs as some reviewers suspect. Moreover, the absorption feature around 325 nm was greatly developed after the temperature reached to 240 °C, hence, some activated precursor "complexes" are responsible for it rather than CdS or ZnS particles. That the obtained QDs are ZnCdS alloy in nature is further evident by their relationship of size-absorption peak position. Figure 3 (right) shows the typical TEM images of the ZnCdS nanocrystals from the 3Zn−1Cd−4S batch with the growth periods of 8, 45, and 180 min at 240 °C. Basically, these ZnCdS nanocrystals are spherical in shape with narrow size distribution; their crystallinity is high as shown in the inset. These 8-, 45-, and 180-min nanocrystals are very much similar in size, with their average diameters of 3.4 ± 0.4, 3.4 ± 0.5, and 3.6 ± 0.5 nm, respectively. Thus, there is no significant increase in size during the 8−180 min growth at 240 °C. It is noteworthy that 3.4−3.6 nm binary CdS QDs exhibit first excitonic absorption peaks at 401−407 nm,[9] whereas our nanocrystals at the same size range exhibit the "fixation" of first excitonic absorption peaks at 402−400 nm. Therefore, our QDs are ZnCdS alloy in nature. Furthermore, these ZnCdS are gradient rather than homogeneous; such a structure is illustrated in detail in the below session.

3.2. Structural Identification and Alloying Mechanism.. It is essential to study the synthesis-structure−property relationship both from the fundamental and application point of view; particularly for ternary QDs, the structural determination of homogeneous vs gradient alloys is challenging and not straightforward. Recently, solid-state magic-angle-spin (MAS) ^{113}Cd, ^{77}Se, ^{13}C, and ^{31}P NMR were successfully used to investigate ternary CdTeSe alloy QDs and a layered CdSe/CdTe/CdSe structure with their surface ligands of tri-*n*-octylphosphine (TOP) and trioctylphosphine oxide (TOPO).[20] From the ^{13}C NMR, it was discovered that these capping ligands were weakly bound to the surfaces of the nanocrystals, and were quite mobile over the surface. The ^{113}Cd NMR provided crucial information to determine the composition and structure of these materials. Solid-state MAS ^{13}C and ^{113}Cd NMR were also used in the current research to investigate the bonding of surface ligands and the composition and structure of the ZnCdS QDs. In addition to solid-state NMR, XPS, TEM, and XRD were also used to characterize the structure of our ternary QDs. These characterization techniques are presented below in the order of XPS, TEM, NMR, and XRD, and the results are summarized in Table 1, together with the band gap absorption and emission peak position and PL fwhm of the crude samples. These QDs were synthesized from feed molar ratios of 0Zn−1Cd−1S, 1Zn−1Cd−1S, 3Zn−1Cd−2S, and 3Zn−1Cd−4S. Furthermore, each 8-min sample studied in this session was synthesized from an individual batch.

3.2.1. XPS and TEM. As shown in Figure 4, XPS was used to determine the atomic compositions of our QDs. The CdS QDs contain no Zn as expected (Table 1). For the $Zn_xCd_{1-x}S$ QDs from the batches with the feed molar ratios of 1Zn−1Cd−1S with 180 min growth, 3Zn−1Cd−2S with 8 and 180 min growth, and 3Zn−1Cd−4S with 8 and 180 min growth, the x values (Zn mole percentage in the total atoms of Cd and Zn) were determined to be 0.13, 0.12, 0.36, 0.52, and 0.66, respectively. It should be mentioned that XPS is a surface-sensitive technique, the depth dependence of the observed signal intensity, I, for the primary X-ray photoemitted electrons, is $I = I_0 \exp(-z/\lambda)$, where z is the distance of the emitting atoms from the sample surface, I_0 is the unattenuated signal intensity, and λ is the (energy and material dependent) attenuation length of the emitted electron.[23] The actual λ value is difficult to determine due to the complex composition of the QDs (containing organic capping layer and mixed ZnS and CdS). There is no doubt the obtained compositions represent the actual values if the particles are homogeneous; the obtained compositions are also reasonably true if slightly inhomogeneous since they are small in size (∼4 nm, Table 1), or at least the sequence of Zn content in various samples is real. We tested one QD ensemble from the feed molar ratio of 3Zn−1Cd−4S with 180-min growth by EDX (energy dispersive X-ray analysis); the results in atomic % are Zn (30.52 ± 3.15)%, Cd (19.08 ± 4.12)%, S (50.40 ± 5.83), i.e., $Zn_{0.62}Cd_{0.38}S_{1.02}$ (the footnote value of S refers the atomic ratio of S to total metals), which is in perfect agreement with $Zn_{0.61}Cd_{0.39}S_{1.16}$ determined by XPS. It is noteworthy that the Zn-to-Cd (molar ratio) in the product is always less than that of the feed molar ratio, which is because the ZnS formation is slower than the CdS formation under the present experimental condition. Meanwhile, the Zn content increases in the resulting ZnCdS QDs with increasing Zn-to-Cd feed molar ratio and S feed amount as well as increaing growth period at 240 °C. For example, during the 8-min growth period, namely the early growth stage, the CdS formation seems to dominate with a little Zn incorporated in the CdS lattice for the synthetic batch with

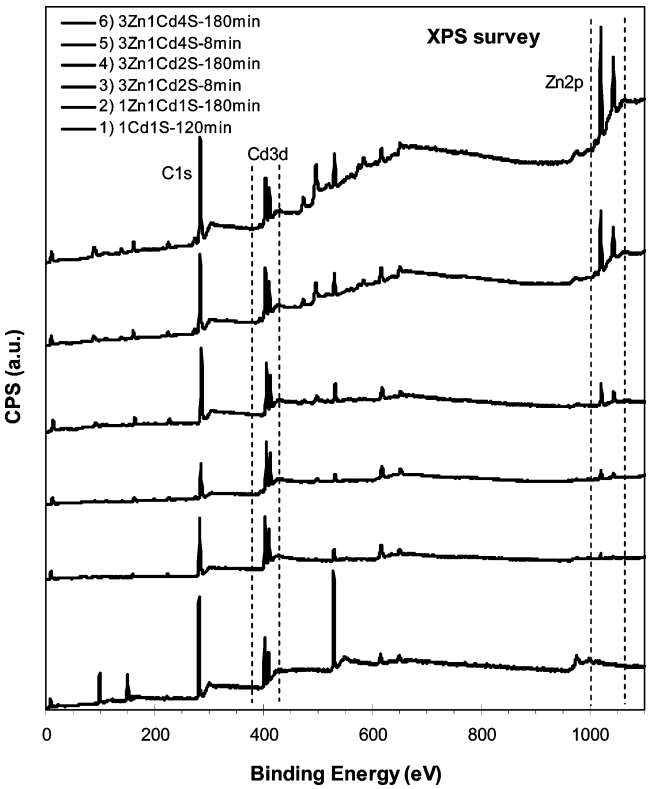

Figure 4. XPS of the nanocrystals from the synthetic batches with the feed molar ratio of (1) 0Zn−1Cd−1S with 120-min growth, (2) 1Zn−1Cd−1S with 180-min growth, (3) 3Zn−1Cd−2S with 8-min growth, (4) 3Zn−1Cd−2S with 180-min growth, (5) 3Zn−1Cd−4S with 8-min growth, and (6) 3Zn−1Cd−4S with 180-min growth. The resulting $Zn_xCd_{1-x}S$ nanocrystals are characterized as (1) CdS, (2) $Zn_{0.13}Cd_{0.87}S$, (3) $Zn_{0.12}Cd_{0.88}S$, (4) $Zn_{0.12}Cd_{0.88}S$, (5) $Zn_{0.52}Cd_{0.48}S$, and (6) $Zn_{0.66}Cd_{0.34}S$. The Cd amounts are calculated from the peaks in the range of 402−416 eV (for Cd 3d), while Zn in the range of 1017−1050 eV (for Zn 2p).

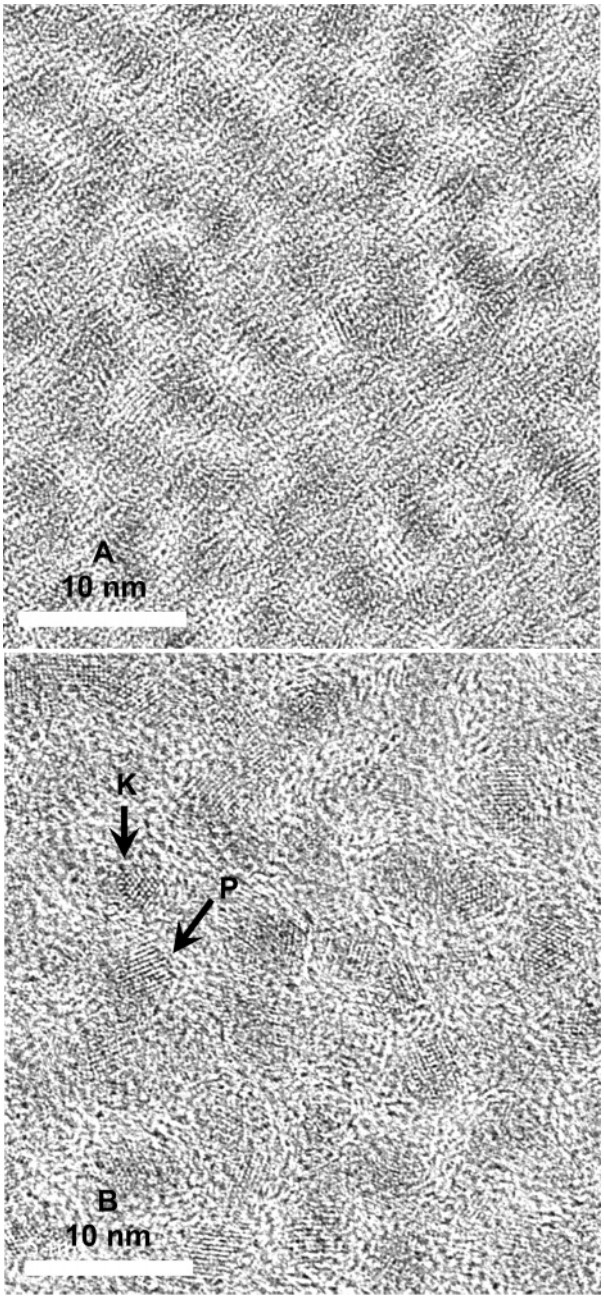

Figure 5. High-resolution TEM images of the nanocrystals from the large-scale syntheses (shown in Table 1). (A) 8-min ZnCdS and (B) 180-minute ZnCdS from the 3Zn−1Cd−4S feed molar ratio. The *d* spacing of the one-dimensional lattice (shown in particle P) is measured to be 3.18 Å; our XRD study presented below (Figure 8) shows that the nanocrystals are cubic in crystal structure. The *d* spacing values of the most prominent plane (111) of bulk zincblende ZnS is 3.12 Å (Joint Committee on Powder Diffraction Standards JCPDS 05−0566) and that of bulk zincblende CdS is 3.36 Å (JCPDS 10−0454).

the 3Zn−1Cd−2S feed molar ratio, while much more Zn in the CdS lattice for the batch with the 3Zn−1Cd−4S feed molar ratio.

The same nanocrystals were imaged by TEM. The nanocrystals appear essentially spherical and uniform in size. Typical high-resolution TEM images are presented in Figure 5, for the ensembles of the 8- and 180-min ZnCdS QDs from the 3Zn−1Cd−4S feed molar ratio. The 8-min ensemble is ca. 3.5 nm in diameter, while the 180-min is ca. 4.1 nm. Both two-dimensional (such as particle K) and one-dimensional (such as particle P) lattice structures are clearly observed, indicating a fair degree

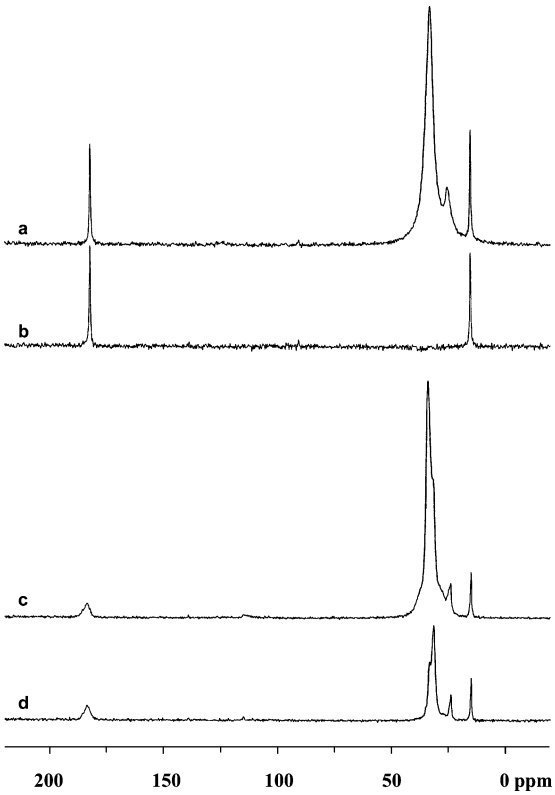

Figure 6. ^{13}C CP/MAS NMR spectra of stearic acid (a) without and (b) with dipolar dephasing, and of the 8-min ZnCdS NCs capped with stearic acid synthesized from the feed molar ratio of 3Zn−1Cd−4S (c) without and (d) with dipolar diphasing.

of crystallinity. Therefore, it is fair to conclude that our ZnCdS nanocrystals are high-quality, regarding crystallinity, spherical shape and distribution, and uniformity in size.

3.2.2. Solid-State MAS NMR. As shown in Figure 6a, the normal ^{1}H-^{13}C cross-polarization CP/MAS NMR spectrum of pure stearic acid ($CH_3-(CH_2)_{16}-COOH$) shows four main features: $-COOH$ at ∼182 ppm, $-CH_3$ at 15.2 ppm, $-CH_2$ adjacent to $-CH_3$ at ∼25.1 ppm, and all the other $-CH_2$ groups (from the α-C through the middle of the chain) fall in the range 30−36 ppm (the distribution peaking at 33 ppm). In the dipolar-dephased (DD) CP/MAS NMR spectrum shown in Figure 6b, only the $-COOH$ and $-CH_3$ resonances remain. The dipolar dephasing experiment shows only those C atoms that are not strongly dipolar-coupled to ^{1}H, namely quaternary carbons and any proton-bearing carbons that are in motion so that their dipolar coupling is reduced.[20] Thus it is clear that the stearic acid molecule in its bulk solid phase is rigidly fixed and the only dynamics possible is the internal rotation of $-CH_3$. The normal ^{13}C CP/MAS NMR spectrum of the 8-min ZnCdS QDs with the surface ligands of stearic acid from the 3Zn-to-1Cd-to-4S batch shown in Figure 6c, which presumably now represents stearate ions, shows strong similarities to the spectrum in Figure 6a, but the peak of $-COO^-$ (183.2 ppm) is noticeably broader and the main peak corresponding to the main backbone of $-CH_2$ groups (at 33.6 ppm) has a significant shoulder (at ∼ 31.5 ppm) and a broad underlying feature (centered at ∼ 32 ppm). The 14.8 ppm peak is from $-CH_3$, while the ∼ 24 ppm peak is from $-CH_2$ adjacent to $-CH_3$. The broadening effects are consistent with a distribution of environments that might be expected on changing to a noncrystalline coating on a nanocrystal.[20] The dipolar dephased spectrum of the QD ensemble, Figure 6d, shows lines in addition to the expected peaks of $-COO^-$ and $-CH_3$, which logically can be assigned

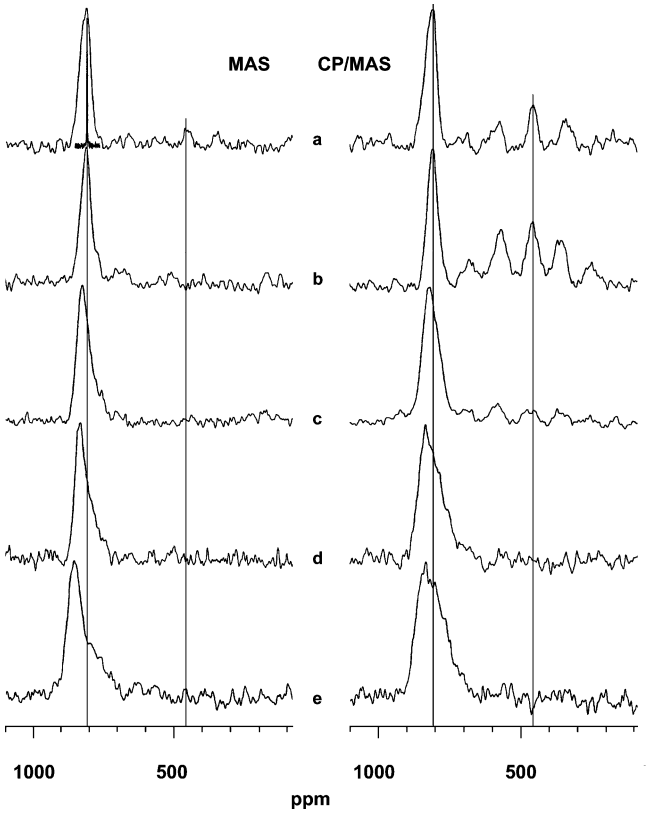

Figure 7. ^{113}Cd MAS NMR spectra (left) and corresponding ^{113}Cd CP/MAS NMR spectra (right), with (a) 180-min CdS NCs (MAS rate 7 kHz (left) and 7.7 kHz (right)), (b) 8-min ZnCdS NCs from the feed molar ratio of 3Zn−1Cd−2S (MAS rate 7.1 kHz), (c) 180-min ZnCdS NCs from 3Zn−1Cd−2S (MAS rate 7.1 kHz), (d) 8-min ZnCdS NCs from 3Zn−1Cd−4S (MAS rate 6.3 kHz (left) and 6.7 kHz (right)), and (e) 180-min ZnCdS NCs from 3Zn−1Cd−4S (MAS rate 7.2 kHz). The much sharper spectrum of bulk Wurtzite CdS is also shown in (a) (left) for comparison.

to the last few $-CH_2$ groups of the chain adjacent to $-CH_3$ undergoing some dynamics, whereas resonances from the $-CH_2$ carbons in the middle of the chain and adjacent to the carboxylate have disappeared from the spectrum, indicating that these must be static. Accordingly, it seems reasonable that the acid molecule is tethered to the surface of the nanocrystal through coordination of the carboxylate, and only the opposite extremities of the chain have some freedom to move. Such a conclusion is in agreement with high-resolution ^1H NMR results on QD liquid dispersions, which show that the surface ligand attaches strongly to the surfaces of the CdS and ZnCdS QDs. For example, little ^1H signal from $-CH_2$ adjacent to $-COO^-$ was observed in the ^1H NMR spectrum of one ensemble of CdS QDs capped with myristic acid ($CH_3-(CH_2)_{12}-COOH$) dispersed in $CDCl_3$, indicating little free surface ligands in the solvent due to the strong attachment of the ligand to the QD surface; this ensemble dispersion was measured again after 2-month storage in the dark under ambient conditions and still no free myristic acid was detected.

Due to the strong attachment of the acid molecule to the QD surface it was possible to obtain ^1H-^{113}Cd CP/MAS NMR spectra, Figure 7-right, which should selectively observe any Cd close to the surface. ^{113}Cd MAS NMR spectra, Figure 7 (left), obtained with single pulse excitation (no CP) should show all Cd. Three aspects are immediately apparent:

First, each of the QD samples features a main peak in the 800^+ ppm region, which is very much broader than the resonance of bulk CdS (hexagonal Wurtzite structure) at 805.7 ppm (shown in Figure 7a (left) for comparison). The broad width of the QD resonance corresponds to a distribution of Cd environments, as discussed previously for CdSe and CdTe QDs.[20d] Note that we do not yet know the chemical shift for bulk cubic CdS. The chemical shift of this main peak increases from 808 to 853 ppm, together with an increase in its overall width and development of a pronounced asymmetry on the low chemical shift side, from the QD sample of the 180-min CdS (Figure 7a-left), to the 8-min (Figure 7b (left)) and 180-min (Figure 7c (left)) ZnCdS from the 3Zn−1Cd−2S batches, and to the 8-min (Figure 7d (left)) and 180-min (Figure 7e (left)) ZnCdS from the 3Zn−1Cd−4S batches. As shown in Table 1 from the XPS study, the Zn content in these corresponding four ZnCdS QD samples increases with the resulting atomic ratio of Zn:Cd as 12:88, 36:64, 52:48, and 66:34. Accordingly, the gradual increase in chemical shift is consistent with the alloying process to form ZnCdS QDs with increasing Zn content, which is similar to the previous observation of an increase of Se content in the CdSeTe QD leading to an increase in chemical shift away from the CdTe resonance and toward that of CdSe.[20] It is noteworthy that increasing ^{113}Cd chemical shift correlates with decreasing lattice constant in the two ternary QD systems, namely CdTeSe and ZnCdS.

Second, a new resonance consisting of an isotropic line at ~457 ppm with several spinning sidebands (ssb) shows quite strongly in the CP spectra of the ensembles of the 180-min CdS (Figure 7a (right)) and 8-min QDs from the 3Zn−1Cd−2S batch (Figure 7b (right)). This resonance is weaker in the CP spectrum of the 180-min QDs from 3Zn−1Cd−2S batch (Figure 7c (right)), and it eventually disappears in the CP spectra of the 8-min (Figure 7d (right)) and 180-min QDs (Figure 7e (right)) from the 3Zn−1Cd−4S batches. As mentioned above, the ^1H-^{113}Cd CP MAS NMR spectra shown in Figure 7 (right) should display Cd atoms in proximity to the protons of the acid chain, namely those Cd atoms at or close to the surface of the nanocrystals. The prominence of the new resonance at 457−458 ppm in the CP spectra of the CdS and ZnCdS QDs with low Zn content suggests that this is the surface Cd to which the ligand $-COO^-$ group is coordinated. The large high-field shifting of this new resonance as compared to that at 800^+ ppm is consistent with increased O coordination: the Cd resonances of bulk Cd salts, such as Cd acetate and Cd myristate, were detected in the 0−60 ppm region; there is likely multiple O coordination in these salts, whereas the nanocrystal surface Cd atoms should have less O coordination because of their existing attachment to the sulfide lattice. The presence of several strong spinning sidebands, which arises from considerable chemical shift anisotropy, also distinguishes this site as being quite asymmetric compared to the roughly tetrahedral CdS_4 sites of the 800^+ ppm resonance, for which no spinning sidebands are visible. It is then evident that the reduction and low-field shifting to ~468 ppm of the 457-ppm resonance for the QDs with long growth periods (such as 180-min growth from the 3Zn−1Cd−2S feed molar ratio) and its disappearance for high S feed batches (such as the 8- and 180-min growth from the 3Zn−1Cd−4S feed molar ratio) is consistent with the displacement of Cd atoms from these stearate-coordinated surface sites by Zn atoms. Furthermore, the Zn concentration at the surface must be higher than that in the nanocrystals as a whole. If the material were homogeneous, then even at a Zn:Cd ratio of 66:34, the stearate-attached Cd should still be visible. The fact that it is invisible attests to depletion of Cd at the surface.

Third, there are differences in the spectra with and without CP in the 800^+ ppm region which become more pronounced as

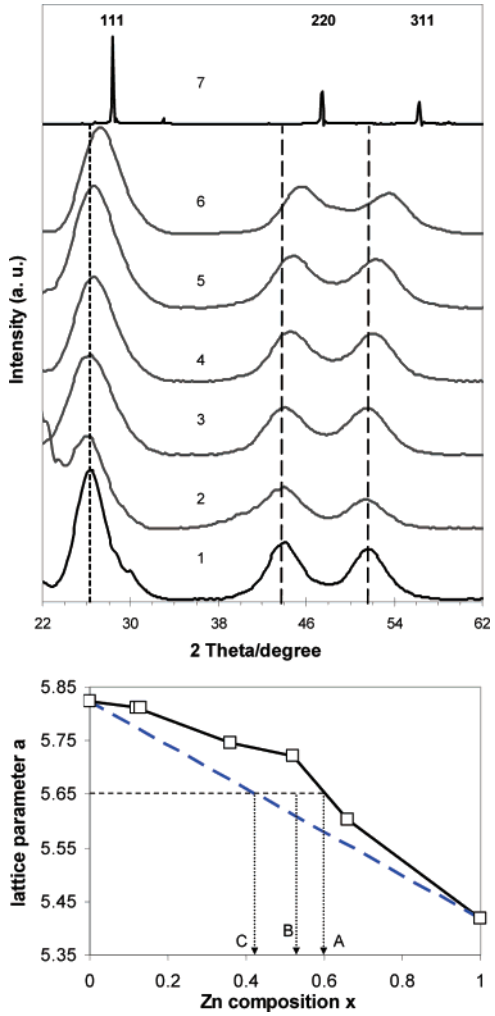

Figure 8. (Top) Powder XRD patterns of the nanocrystals from the synthetic batches with the feed molar ratio of (1) 0Zn−1Cd−1S with 120-min growth, (2) 1Zn−1Cd−1S with 180-min growth, (3) 3Zn−1Cd−2S with 8-min growth, (4) 3Zn−1Cd−2S with 180-min growth, (5) 3Zn−1Cd−4S with 8-min growth, (6) 3Zn−1Cd−4S with 180-min growth, and (7) bulk cubic ZnS. The resulting $Zn_xCd_{1-x}S$ nanocrystals from the noninjection approach were characterized by XPS as (1) CdS, (2) $Zn_{0.13}Cd_{0.87}S$, (3) $Zn_{0.12}Cd_{0.88}S$, (4) $Zn_{0.12}Cd_{0.88}S$, (5) $Zn_{0.52}Cd_{0.48}S$, and (6) $Zn_{0.66}Cd_{0.34}S$. The dashed lines are for eye guidance. (Bottom) The dependence of the lattice parameter *a* (in Å, □) of the synthesized $Zn_xCd_{1-x}S$ nanocrystals on the Zn molar composition *x* determined by XPS. The lattice parameter *a* was calculated from the XRD patterns shown in Figure 8, top (based on 220 diffraction). The blue dashed linear line represents the Vegard's law. The other black dashed lines and points A, B, and C illustrate an assumption of the *a*−*x* relationship as described in text.

the concentration of Zn in the QD sample increases: A broad peak is still observed in the 800^+ ppm region in all the CP spectra, and this must represent near-surface Cd atoms probably still largely coordinated by 4S in a roughly tetrahedral coordination. As such they represent only a fraction of the total Cd in the QDs. The asymmetric high-field broadening which develops in the non-CP spectra as the Zn level in the nanocrystal increases is even more pronounced in the CP spectra, with the most obvious in the spectrum of the 180-min QDs from the 3Zn−1Cd−4S batch. Since the alloyed ZnCdS QDs exhibit higher ^{113}Cd NMR chemical shifts than CdS, the origin of such a high-field broadening is puzzling; however, since such broadening in the CP spectra is associated with increasing Zn at the surface, it is speculated that these may be near-surface CdS_4 centers which are linked to surface Zn. This would be consistent with an inhomogeneous distribution of Zn in the ZnCdS QDs.

3.2.3. XRD. Figure 8 (top) shows the XRD patterns of the ZnCdS QDs from the large-scale noninjection syntheses. The XRD patterns indicate that the nanocrystals have a cubic crystal structure, with the absence of the (102) and (103) diffraction peaks existing in a hexagonal crystal structure. It was reported that the ZnCdS QDs via a hot-injection approach with the growth at 260 °C have a cubic crystal structure,[13] while at 300 °C have a hexagonal crystal structure.[18] However, this temperature effect does not apply in our approach: the CdS QDs growing at 300 °C still reveals a cubic crystal structure.

Assuming there is no microstrain in the nanocrystals, the average sizes of the nanocrystal ensembles are estimated from the Sherrer equation[24] (Table 1). Such an assumption should lead to inaccuracy in the size estimation for the ternary ZnCdS QDs, because the Cd−S and Zn−S bond lengths are different. If the presence of the microstrain[25] is considered for the ZnCdS QDs, the estimated size should be larger than that listed in Table 1; however, the present study does not further address such an issue on the size estimation from XRD. It is interesting to point out that based on the XRD study with the Sherrer equation,[24] the size of the CdS ensemble was calculated to be 4.90 nm, which is in good agreement with that, 4.85 nm, estimated from the band gap absorption peak position at 440 nm;[10b] however, 4.90 nm is larger than 4.2 nm measured from TEM. As shown in Table 1, there is a difference in sizes determined from XRD and TEM, for one identical QD ensemble.

It is acknowledged that homogeneous ternary alloys obey Vegard's law of linear relationships between the lattice parameters and compositions of solid-solution alloys,[26] with the composition expressed as atomic percentage.[18] As shown in Figure 8 (top), the diffraction peaks shift to the direction of larger Bragg angle with an increase of the Zn content in the samples. Such an increase in 2θ indicates that Zn atoms are gradually incorporated into the CdS lattice leading to the formation of the ZnCdS QDs with an increase of the Zn content along the growth and a decrease in their lattice parameters. Figure 8 (Bottom) shows the relationship between the lattice parameter *a* calculated from the (220) diffraction and the Zn composition *x* determined by XPS; clearly, such a relationship does not comply with Vegard's law.[18,26] The calculated *a* value is larger than that from Vegard's law with the same Zn content in the ternary ZnCdS materials. CdS has a larger *a* than ZnS does; the departure from the linear relationship of Vegard's law indicates that the obtained ZnCdS alloyed QDs are not homogeneous in structure. Concerns may be raised regarding to the validity of such an *a*−*x* relationship due to the suspicious inaccuracy of **x** values determined by XPS. To answer this question, we make an assumption as depicted in Figure 8 (bottom): assuming Zn composition denoted at point A is overestimated because of XPS surface sensitivity (Zn is rich in surface from solid NMR analysis), the real Zn composition can vary between point A to point C (point C exclusive; C means homogeneous structure, in the case of which, overestimation of Zn is invalid), for instance, at point B, thus there are only differences in the deviation extent, but the departure of the *a*−*x* relationship from Vegard's law is still valid. In addition to the above-mentioned, another evidence of alloying was suggested by our PL lifetime study,[27] which shows that the 120-min CdS ensemble as well as the 180-min ZnCdS ensemble from 1Zn−1Cd−1S and 3Zn−1Cd−4S feed molar ratios exhibit different PL lifetime and upconversion photoluminescent lifetime.

Subsequently, a plausible alloying mechanism for the growth of the ZnCdS nanocrystals via our noninjection approach is proposed: a Cd-rich core is initially formed due to a higher reactivity of Cd than Zn toward S, leading to the redshift of band gap absorption and emission in the initial/early growth stage. Afterward, there is a gradual formation of Zn-rich outer layers because of the rapid depletion of the Cd concentration in the reaction medium leading to the excess of Zn (and S); also the outer layers have an increase in the zinc content toward the surface. Furthermore, the outermost layer may mainly consist of ZnS with little cadmium, as seen from the samples synthesized with high Zn-to-Cd feed molar ratio and high S feed amount. Such an accumulation of ZnS in the outer layers directly leads to an effective inorganic 'coating' to well protect the CdS-rich core, giving rise to the observed 'fixation' of band gap absorption and emission, and resulting the enhanced UV resistance and storage stability of the nanocrystals (see the Supporting Information). At the later growth stage, Zn may diffuse into the inner CdS-rich core, leading to the blueshift of the band gap absorption and emission.

4. Conclusions

The present study focuses on the synthesis-structure−property relationships of ternary ZnCdS alloys. Colloidal photoluminescent ZnCdS QDs were readily synthesized via a noninjection approach. Such a "green" chemistry approach uses air-stable chemicals under mild reaction conditions, with great reproducibility and large-scale capability for high-quality ternary ZnCdS QDs with controllable bandgaps. The growth of the ternary nanocrystals is sensitive to the Zn−Cd−S feed molar ratio. The fixation of the band gap absorption and emission is characteristic for the synthetic conditions with high feed amounts of Zn and S. The ZnCdS nanocrystals have a cubic crystal structure and are inhomogeneous with Cd-rich inner cores and Zn-rich outer layers. The gradient structure was evidenced by solid state ^{113}-Cd NMR and XRD. The ternary ZnCdS QDs, with intense PL emission and narrow fwhm, are excellent candidates as blue-luminescent materials for various applications.

Acknowledgment. The authors would like to thank Mr. Don Leek for his help in ^{1}H high-resolution NMR study and useful discussion.

Supporting Information Available: The detail purification procedure, the summary of growth kinetics and optical properties from five different Zn−Cd−S feed molar ratios, and the photo- and storage-stability results. This material is available free of charge via the Internet at http://pubs.acs.org.

References and Notes

(1) Alivisatos, A. P. *Science* **1996**, *271*, 933−937.

(2) Coe-Sullivan, S.; Woo, W.-K.; Steckel, J. S.; Bawendi, M.; Bulović, V. *Org. Electron.* **2003**, *4*, 123−130.

(3) (a) Chan, W. C. W.; Nie, S. *Science* **1998**, *281*, 2016−2018. (b) Michalet, X.; Pinaud, F. F.; Bentolila, L. A.; Tsay, J. M.; Doose, S.; Li, J. J.; Sundaresan, G.; Wu, A. M.; Gambhir, S. S.; Weiss, S. *Science* **2005**, *307*, 538−544. (c) Medintzi, I. L.; Uyeda, H. T.; Goldman, E. R.; Mattoussi, H. *Nat. Mater.* **2005**, *4*, 435−446.

(4) (a) Murray, C. B.; Norris, D. J.; Bawendi, M. G. *J. Am. Chem. Soc.* **1993**, *115*, 8706−8715. (b) Dabbousi, B. O.; Rodriguez-Viejo, J.; Mikulec, F. V.; Heine, J. R.; Mattoussi, H.; Ober, R.; Jensen, K. F.; Bawendi, M. G. *J. Phys. Chem. B* **1997**, *101*, 9463−9475. (c) Peng, Z. A.; Peng, X. *J. Am. Chem. Soc.* **2001**, *123*, 183−184. (d) Xie, R.; Kolb, U.; Li, J.; Basché, T.; Mews, A. *J. Am. Chem. Soc.* **2005**, *127*, 7480−7488. (e) Yang, Y. A.; Wu, H.; Williams, K. R.; Cao, Y. C. *Angew. Chem., Int. Ed.* **2005**, *44*, 6712−6715.

(5) (a) Yu, K.; Singh, S.; Patrito, N.; Chu, V. *Langmuir* **2004**, *20*, 11161−11168. (b) Kalyuzhny, G.; Murray, R. W. *J. Phys. Chem. B* **2005**, *109*, 7012−7021. (c) Jasieniak, J.; Mulvaney, P. *J. Am. Chem. Soc.* **2007**, *129*, 2841−2848.

(6) (a) Manna, L.; Scher, E. C.; Li, L. S.; Alivisatos, A. P. *J. Am. Chem. Soc.* **2002**, *124*, 7136−7145. (b) Yu, K.; Zaman, B.; Singh, S.; Wang, D.; Ripmeester, J. A. *J. Nanosci. Nanotechnol.* **2005**, *5*, 659−668. (c) Yu, K.; Zaman, B.; Ripmeester, J. A. *J. Nanosci. Nanotechnol.* **2005**, *5*, 669−681. (d) Yu, K.; Zaman, B.; Singh, S.; Wang, D.; Ripmeester, J. A. *Chem. Mater.* **2005**, *17*, 2552−2561.

(7) (a) Eichkorn, K.; Ahlrichs, R. *Chem. Phys. Lett.* **1998**, *288*, 235−242. (b) Lopez del Puerto, M.; Tiago, M. L.; Chelikowsky, J. R. *Phys. Rev. Lett.* **2006**, *97*, 096401(1−4).

(8) Hernandez-Calderon, I. *II-VI Semiconductor Materials and Their Applications*, (Ed. Tamargo, M. C.), P136−138, Vol. 12 in *Optoelectronic Properties of Semiconductors and Superlattices*; Manasreh, M. O., Ed.; Taylor & Francis Inc.: New York, 2002.

(9) Rama Krishna, M. V.; Friesner, R. A. *J. Chem. Phys.* **1991**, *95*, 8309−8322.

(10) (a) Vossmeyer, T.; Katsikas, L.; Giersig, M.; Popovic, I. G.; Diesner, K.; Chemseddine, A.; Eychmüller, A.; Weller, H. *J. Phys. Chem.* **1994**, *98*, 7665−7673. (b) Yu, W. W.; Qu, L.; Guo, W.; Peng, X. *Chem. Mater.* **2003**, *15*, 2854−2860. (c) Yu, K.; Ouyang, J.; Vincent, M.; Chabloz, D.; Wilkinson, B.; Perier, F. *Doped Nanomaterials and Nanodevices*; Chen, W., Ed.; American Scientific Publishers: Stevenson Ranch, CA, 2007.

(11) Yoffe, A. D. *Adv. Phys.* **1993**, *42*, 173−266.

(12) Yu, W. W.; Peng, X. *Angew. Chem., Int. Ed.* **2002**, *41*, 2368−2371.

(13) Zhong, X.; Liu, S.; Zhang, Z.; Li, L.; Wei, Z.; Knoll, W. *J. Mater. Chem.* **2004**, *14*, 2790−2794.

(14) Cao, Y. C.; Wang, J. *J. Am. Chem. Soc.* **2004**, *126*, 14336−14337.

(15) Peng, X. *Chem. Eur. J.* **2002**, *8*, 334−339.

(16) Spanhel, L.; Haase, M.; Weller, H.; Henglein, A. *J. Am. Chem. Soc.* **1987**, *109*, 5649−5655.

(17) Wang, W.; Germanenko, I.; EI-Shall, M. S. *Chem. Mater.* **2002**, *14*, 3028−3033.

(18) Zhong, X.; Feng, Y.; Knoll, W.; Han, M. *J. Am. Chem. Soc.* **2003**, *125*, 13559−13563.

(19) Eaton, D. F. *Pure Appl. Chem*, **1988**, *60*, 1107−1114.

(20) Ratcliffe, C. I.; Yu, K.; Ripmeester, J. A.; Zaman, M. B.; Badarau, C.; Singh, S. *Phys. Chem. Chem. Phys.* **2006**, *8*, 3510−3519.

(21) (a) Jang, E.; Jun, S.; Pu, L. *Chem. Commun.* **2003**, 2964−2965. (b) Swafford, L. A.; Weigand, L. A.; Bowers, II, M. J.; McBride, J. R.; Rapaport, J. L.; Watt, T. L.; Dixit, S. K.; Feldman, L. C.; Rosenthal, S. J. *J. Am. Chem. Soc.* **2006**, *128*, 12299−12306. (c) Bailey, R. E.; Nie, S. *J. Am. Chem. Soc.* **2003**, *125*, 7100−7106. (d) Zhong, X.; Han, M.; Dong, Z.; White, T. J.; Knoll, W. *J. Am. Chem. Soc.* **2003**, *125*, 8589−8594. (e) Zhong, X.; Zhang, Z.; Liu, S.; Han, M.; Knoll, W. *J. Phys. Chem. B* **2004**, *108*, 15552−15559.

(22) Regarding the present synthetic approach, the formation of the ZnCdS nanocrystals is greatly affected by the Zn−Cd−S feed molar ratio and the concentration of the acid used. The acid is sometimes termed as "ligand". The effect of the ligand concentration on the formation of CdS QDs via our noninjection approach was investigated; our results, which, in general, reveal an increase of growth rate in crystal size and a reduction in crystal number with increasing concentration of the used acid, will be presented in a forthcoming manuscript dealing with the precise control of the optical properties, size, and size distribution of the resulting CdS-based QDs via noninjection approaches.

(23) Hoener, C. F.; Allan, K. A.; Bard, A. J.; Campion, A.; Fox, M. A.; Mallouk, T. E.; Webber, S. E.; White, J. M. *J. Phys. Chem.* **1992**, *96*, 3812−3811.

(24) Scherrer, P.; Göettingen, N. G. W. *Math.-Physik. Klasse* **1918**, 98.

(25) Kokanović, I.; Tonejc, A. *Mater. Sci. Eng. A* **2004**, *373*, 26−32.

(26) (a) Vegard, L. Z. *Z. Physik* **1921**, *5*, 17−26. (b) Vegard, L. Z. *Z. Kristallogr.* **1928**, *67*, 239. (c) Furdyna, J. K. *J. Appl. Phys.* **1988**, *64*, R29−64.

(27) Ouyang, J.; Ripmeester, J. A.; Wu, X.; Kingston, D.; Yu, K.; Joly, A. G.; Chen, W. *J. Phys. Chem. C* **2007**, *111*, 16261−16266.